Confined Bilayers Passively Regulate Shape and Stress

Margarita Staykova,[1,*] Marino Arroyo,[2,†] Mohammad Rahimi,[2] and Howard A. Stone[1]
[1]*Department of Mechanical and Aerospace Engineering, Princeton University, Princeton, New Jersey 08544, USA*
[2]*LaCàN, Universitat Politècnica de Catalunya BarcelonaTech, Barcelona 08034, Spain*

Lipid membranes are commonly confined to adjacent subcellular structures or to artificial substrates and particles. We develop an experimental and theoretical framework to investigate the mechanics of confined membranes, including the influence of adhesion, strain, and osmotic pressure. We find that supported lipid bilayers respond to stress by nucleating and evolving spherical and tubular protrusions. In cells, such transformations are generally attributed to proteins. Our results offer insights into the mechanics of cell membranes and can further extend the applications of supported bilayers.

Biological membranes are dynamical interfaces that undergo continual remodeling, usually by cytoskeleton-induced forces [1], by tuning locally the lipid composition, or through interactions with specialized proteins [2]. In this Letter, we characterize a generic mechanical mechanism by which stressed membranes delaminate from their confining structure to form stable, highly curved tubular and spherical protrusions. In biomimetic systems, protrusions form out of confined membranes upon straining the membrane-supporting surface [3,4] or upon incorporating lipids or peptides in supported bilayers [5–7]. Similar processes have been observed in cells, where the plasma membrane bulges into blebs [8] and microvesicles [9] upon contraction of the underlying actin cortex, or forms tubular invaginations away from the substratum in shrinking adherent cells [10]. We provide a unified view of these phenomena and investigate the behavior of confined membranes with experiments, theory, and simulations.

For the experiments, we construct a channel between a glass cover slip and a polydimethylsiloxane (PDMS) slab, and we coat it with a uniform lipid bilayer composed of 1,2-dioleoyl-sn-glycero-3-phosphocholine (DOPC) and fluorescently labeled with 1 mol % 1,2-dipalmitoyl-sn-glycero-3-phosphoethanolamine-*N*-(lissamine rhodamine B sulfonyl) (ammonium salt) (Rh-DPPE) (see procedure in Ref. [3]). The PDMS slab contains an additional cylindrical puncture (1 mm in diameter) between the inlet and outlet, which is covered by a thin PDMS sheet (about 100 μm thick), and connected at the other end to a microsyringe pump [Fig. 1(a)]. Initially, both the solution in the channel and the few nanometer thick interstitial liquid film, which separates the membrane from the substrate [11], are at the osmolarity at which the bilayer is prepared ($M_0 = 0.3$ Osm). Using this original setup, we can (1) subject a supported lipid membrane to a lateral strain by deforming (inflating or deflating) the PDMS sheet underneath the membrane [3] and (2) modify the volume of interstitial liquid by controlling the osmolarity of the solution above the membrane [12].

Our confocal observations reveal that single-component supported bilayers in the fluid phase exhibit different morphologies, a uniform state or states with tubular or spherical lipid protrusions, which can be controlled reversibly by the magnitude of the applied strain and the interstitial volume [Fig. 1(b)]. Moreover, we will demonstrate that highly curved tubules protruding from confined bilayers remain stable, even without the assistance of commonly appreciated mechanisms, such as localized forces [13] or spontaneous curvature [14,15].

To understand the experimental observations, we develop a theoretical model (see Supplemental Material [16]) for the confined bilayer in equilibrium. We idealize

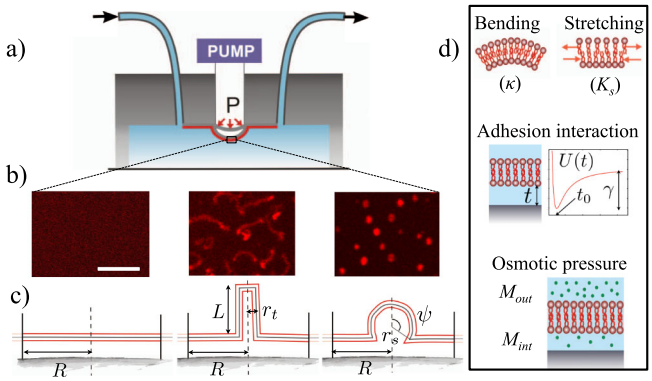

FIG. 1 (color online). (a) Experimental setup. (b) Confocal observations show three main membrane morphologies (scale bar: 5 μm). (c) Corresponding model idealizations as a uniform membrane disc with radius R; or discs with a tubular (radius r_t, length L) or a spherical protrusion (radius r_s, contact angle ψ). The free energy of these three families of shapes includes the contributions shown in (d), with the corresponding material properties; $K_s = 0.12$ J/m^2 is the elastic compressibility modu lus of each monolayer; $\kappa = 10^{19}$ J is the bending modulus [29]; for U, we adopt the functional form proposed in Ref. [11] with an equilibrium separation $t_0 = 3$ nm and set the adhesion energy to $\gamma = U(+\infty) \quad U(t_0) = 2$ mJ/m^2 estimated from the lysis of shallow caps (see text).

the membrane as a collection of juxtaposed cells with one protrusion at the center of each, which allows us to focus on a single cell of radius R_0 commensurate to half of the average distance between protrusions. In our model, the bilayer adopts the state of lowest free energy amongst three predefined families of shapes, planar, tubular, or spherical [Fig. 1(c)], consistent with our experimental observations and with simulations allowing for general shapes and density distributions (see Supplemental Material [16] and Ref. [17]). For each protrusion mode, the equilibrium state is given by the competition between bending and stretching elastic energies and $U(t)$, the poorly characterized bilayer-substrate interaction potential, which is a function of the separation t [Fig. 1(d)]. The competition between the energy terms is arbitrated by the substrate area, relative to a fixed number of lipids, and by the volume enclosed between the membrane and the substrate. We define the relative area change, or areal strain, upon compression as $\varepsilon_C = -(S - S_0)/S_0 = -(R^2 - R_0^2)/R_0^2$, where S_0 is the relaxed area of the bilayer cell, S is its deformed projected area, and R is half of the mean separation between protrusions after deformation. The enclosed fluid volume is nondimensionalized as $v = V/V_0$, where V_0 is the liquid volume enclosed by a uniformly adhered bilayer cell at its equilibrium lipid density and separation distance. In addition to the equilibrium membrane shape, our model yields the bilayer tension as a sum of the monolayer contributions, $\sigma = \sigma^+ + \sigma^-$, and the mechanical pressure difference across the bilayer, which is required to maintain a given v and defined as $\Delta p_{\mathrm{mech}} = P_{\mathrm{in}} - P_{\mathrm{out}}$. In equilibrium, Δp_{mech} must be balanced by the osmotic pressure difference

$$\Delta p_{\mathrm{osm}} = RT\left(\frac{M_0}{v} - M_{\mathrm{out}}\right), \tag{1}$$

where R is the gas constant, T is the absolute temperature, and M_{out} is the channel osmolarity [Fig. 1(d)].

We find that the planar adhered configuration is never the state of lowest energy for $\varepsilon_C > 0$ and $v > 1$, yet it is experimentally observed for small ε_C and v. This fact, together with our numerical simulations (Supplemental Material [16]), suggests that the planar state is metastable in a region whose boundary can be estimated by linear stability analysis. Our predictions of the onset of buckling agree well with the measured critical strain of $\varepsilon_C \approx 0.08$, for $v \approx 1$ [3].

We organize our experimental and theoretical observations on the membrane morphologies in a strain-volume (ε_C, v) phase diagram (Fig. 2), which also depends on the separation R between the protrusions. For small ε_C and v, the lipid membrane is in a planar, adhered configuration (black region). As we increase ε_C, the uniform membrane buckles and expels tubular protrusions (white region). The tubes appear thin (radii of a few tens of nm) and long (about 100 μm) for small v and large ε_C [Fig. 2(i)]

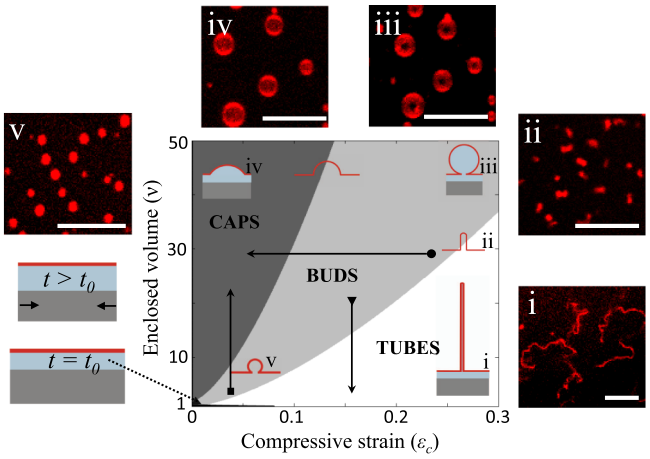

FIG. 2 (color online). Morphological strain volume phase diagram of confined lipid bilayers, derived theoretically for $R_0 = 4$ μm (a typical average half distance between the protrusions in the experiments). We distinguish between a fully adhered planar bilayer (black region) and a bilayer with tubular protrusions, labeled TUBES (white area), or with spherical protrusions, labeled BUDS (light gray) and CAPS (dark gray). Buds ($\pi/2 \leq \psi < \pi$) range between almost full spheres (iii) and half spheres, whereas caps ($\psi < \pi/2$) are shallower spherical protrusions (iv). Buds and caps can be distinguished by the neck opening, which appears as a dark center in the confocal images of the protrusions. The arrows on the diagram map actual experimental paths between tubes, buds, and caps, at R_0 close to 4 μm; for example, filled upward triangle and filled square represent the transitions in Fig. 4, and filled circle represents the transition from image (iii) to (iv). Scale bars are 10 μm. According to the model, along the tube bud boundary $r_s \approx R_0\varepsilon_c^{1/2}/2$ and $v \approx 1 \quad \varepsilon_c + R_0\varepsilon_c^{3/2}/(6t_0)$, which allows us to estimate the strain and volume by estimating r_s and R_0 from the experimental images.

(Supplemental Material [16]). As we increase v, the tubes become thicker and shorter [Fig. 2(ii)] and eventually transform into spherical buds [see also Fig. 4(b)], which are almost complete spheres ($\psi \approx \pi$), with a diameter growing along the tube-bud boundary [Figs. 2(iii) and 2(v)]. As we increase v or decrease ε_C, the contact angle [Fig. 1(c)] of the buds progressively decreases and the neck radius increases, leading to shallow caps [Fig. 2(iv)]. The equilibrium membrane shapes at $\Delta p_{\mathrm{mech}} = \Delta p_{\mathrm{osm}}$ can be mapped onto an alternative phase diagram in terms of ε_C and M_{out} using Eq. (1) (see Supplemental Material [16]). Since we cannot control the nucleation sites of the protrusions in the current setup and, therefore, the distance between them [18], we cannot expect a full quantitative agreement between the experiment and the theory. For instance, the shape transitions in the experiments do not occur in perfect synchrony for all protrusions, and their size may slightly vary depending on the density of the protrusions.

We turn now to the mechanical state of the system and show how confined bilayers are able to passively regulate

stresses, the bilayer tension (σ) and trans-bilayer pressure (Δp), by forming out-of-plane protrusions. In the black region (Fig. 2), the metastable planar adhered bilayer can withstand high negative tension due to the stabilizing effect of adhesion. However, as the substrate contracts, the incompressible liquid film becomes thicker ($t > t_0$) and pressurized ($\Delta p = U'(t) > 0$), and eventually the adhesion is destabilized. By forming protrusions, the system relieves the accumulated σ and Δp [Figs. 3(a) and 3(b)].

The mechanics of protruded states emerge from the energy competition in different ways across the phase diagram. Around the tube-bud phase boundary, the protrusions are near spheres with little penalty in their elastic and adhesion energies. If the volume to area ratio of the protrusions [19] is increased, stretching and adhesion compete, and the spherical protrusions become increasingly shallow and tense, following a Young-Dupre equation $\sigma \approx \gamma/(1-\cos\psi)$. Experimentally, we observe that shallow caps lyse, expelling part of their enclosed volume, and then heal to a state of lower membrane tension [Fig. 3(c)]. This observation provides us with an estimate for the adhesion energy of few mJ/m^2, which is consistent with literature reports on bilayer-glass adhesion [20,21]. If instead the volume becomes scarce, the system accommodates the excess area by forming long thin tubes, stabilized by a negative Δp, and experiencing significant negative σ satisfying $\Delta p \approx \sigma/r_t - \kappa/(2r_t^3)$ [22], in contrast to usual bilayer tubes under tension [13]. In agreement with previous reports [6,23], we observe that tubular protrusions thin out (according to our model, to a radius of 10 nm and a negative membrane tension of a few mN/m), collapse, and detach after a strong hyperosmotic shock (rapid decrease in v) (Supplemental Material [16]), leading to a relaxation of

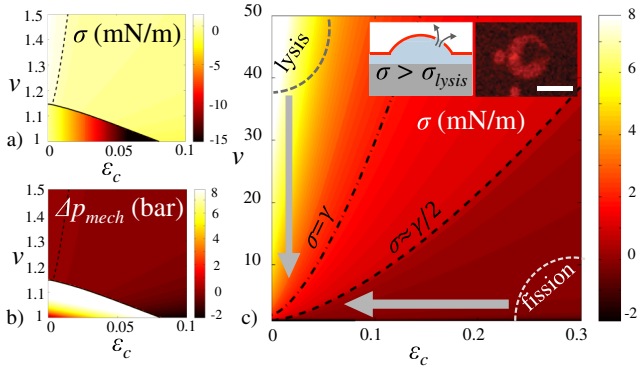

FIG. 3 (color online). Confined bilayers self regulate stress. Numerical plots of (a) bilayer tension and (b) interstitial pressure, as displayed near the planar state of the phase diagram. (c) Numerical plot of the bilayer tension in the protrusions over the entire phase diagram. The regions in the diagram where we observe and theoretically predict shallow caps lysis and thin tubes detachment from the membrane (fission) are indicated, whereas the relaxation of the membrane tension accompanying these events is depicted by gray arrows. The inset shows a sketch and a confocal micrograph of the cap lysis; scale bar = 2 μm.

the membrane tension as the strain is effectively reduced [Fig. 3(c)]. Thus, the confined membrane is able to further self-regulate its pressure and tension by disrupting the bilayer in the highly stressed protrusions.

We note that the negative Δp stabilizing thin tubes arises from a negative osmotic imbalance between the interstitial liquid and the external medium. Indeed, even in nominally iso-osmotic conditions ($M_{\rm out} = M_0$), the tendency of highly curved tubes to dilate and relax their bending energy is readily balanced by the significant dilution of the minute interstitial volume, which occurs even after a slight tube dilation.

Common observations on cells show that the volume of the membrane protrusions changes dynamically due to the semipermeable nature of the lipid membrane and the porosity of the confining structure. To examine the dynamical effects associated with changing v, we subject the membrane to a hypo- (increasing v) or hyperosmotic (decreasing v) outer solution (Supplemental Material [16]). An imbalance between $\Delta p_{\rm osm}(v)$, given in Eq. (1), and $\Delta p_{\rm mech}(\varepsilon_c, v)$, required to stabilize a protrusion at a given volume, drives water into or out of the interstitial space. The volume dynamics is given by

$$\dot{V} = \frac{P_f V_w S_m}{RT}[\Delta p_{\rm osm}(v) - \Delta p_{\rm mech}(\varepsilon_c, v)], \qquad (2)$$

where P_f is the osmotic water permeation coefficient [24,25], V_w is the volume of a water molecule, and S_m is the surface area of the semipermeable membrane. In hypo-osmotic conditions, we observe that the apparent diameter of most buds grows monotonically (vertical paths in Fig. 2) until an equilibrium plateau [Fig. 4(a), filled circle]. For such a protrusion in an homogeneous environment, and estimating ε_C and v as described in Fig. 2, the agreement between experiment and theory is excellent. The buds accommodate their expanding volume (v increases from 3.5 to 22 according to the model) at fixed excess area by flattening into shallow caps and by membrane delamination in the neck region [Fig. 4(a), i–iv]. However, as discussed above [Fig. 3(c)], the volume expansion of the buds at a fixed surface area is accompanied by an increase in the membrane tension. If $\sigma_{\rm lysis}$ is reached in samples with smaller area available for the protrusions (smaller ε_C) and large v, the caps may undergo transient lysis and partially expel their contents [Fig. 4(a), filled square]. Alternatively, we also observe experimentally a collective mechanism of tension relief by coarsening, where smaller caps disappear at the expense of growing spherical protrusions with increasing contact angle ψ [Fig. 4(a), filled upward triangle].

The dynamical transformations of tubes under volume changes are shown in Fig. 4(b). In moderate hyperosmotic conditions, tubes elongate in the first 100 s and then reach a plateau [Fig. 4(c), filled circle], whereas in a stronger hyperosmotic shock, the elongation proceeds more rapidly

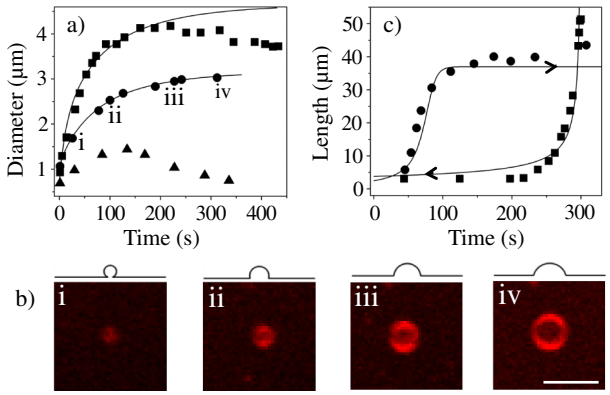

FIG. 4 (color online). Volume dynamics of membrane protru sions upon osmotic changes, determined both experimentally (symbols) and theoretically (lines). (a) Volume dynamics of buds in hypo osmotic conditions (upon complete dilution of the outer solution): gradual bud inflation up to a plateau (filled circle), partial bud lysis (filled square), or bud annihilation by coarsening of the protrusion pattern (filled upward triangle). For the theo retical fits, the initial values for ε_C and v are obtained using the relations shown in Fig. 2 and $P_f \approx 45\ \mu$m/s, measured for DOPC in tension [24]. (b) Snapshots of gradual bud inflation visualized by confocal images (scale bar $= 5\ \mu$m) and the cor responding theoretical profiles. (c) Reversible tube transforma tions, fitted with $P_f \approx 0.75\ \mu$m/s: a gradual bud elongation into a tube (filled circle) in hyperosmotic conditions (increase in external osmolarity from very dilute to 0.2 Osm) and a tube to bud retraction (filled square) upon diluting the outer solution (from 0.6 Osm to water). Shape transitions labeled with (filled circles) on (a) and (c) are mapped on Fig. 2, by the arrows with triangle and square, respectively.

and leads to tubes collapse and detachment, as discussed previously [Fig. 3(c)]. In hypo-osmotic conditions, tubes are converted into buds [Fig. 4(c), filled square]. Theoretically, we can fit the tube dynamics by using a permeation coefficient 60 times smaller than the one used in Fig. 4(a) or reported for DOPC vesicles under tension [24]. We rationalize the reduced water permeation by the decreased area per lipid in the tubes under negative tension, consistent with previous experiments on bilayers of different composition [25]. To our knowledge, these are the first observations showing that the membrane perme- ability can be controlled by the strain.

We have shown that supported bilayers form a variety of protrusions, whose shapes can be experimentally controlled and quantitatively understood in terms of the bilayer-substrate mechanics. The proposed mechanisms do not depend on the previously studied effects of bilayer asymmetry or spontaneous curvature by proteins [2,26]. In fact, passive mechanical and protein-regulated transformations of membranes may act in concert. Our results provide a mechanistic interpretation of the initiation and growth of blebs [8,27], tubular invaginations [10], and microvesicles in cells [9]. Since our experimental system offers a high degree of control, generating a diversity of shapes and lipid densities, it is an ideal workbench to study protein affinity to curvature and lipid packing [28]. Our findings could also help engineer new functionalities into drug delivery systems, such as strain- or pressure-responsive bilayer coated particles.

M. S. and M. A. contributed equally to this work. M. S. and H. A. S. thank Princeton University and the NSF (DMS-1219366) for financial support. M. A. and M. R. acknowledge the support of the European Research Council (FP7/2007-2013, Grant No. 240487), and M. A. acknowledges support through the prize "ICREA Academia" by the Generalitat de Catalunya.

*Staykova@princeton.edu
†Marino.Arroyo@upc.edu

[1] C. Revenu, R. Athman, S. Robine, and D. Louvard, Nat. Rev. Mol. Cell Biol. **5**, 635(2004).
[2] H. T. McMahon and J. L. Gallop, Nature (London) **438**, 590 (2005).
[3] M. Staykova, D. P. Holmes, C. Read, and H. A. Stone, Proc. Natl. Acad. Sci. U.S.A. **108**, 9084 (2011).
[4] Q. Saleem, B. Liu, C. C. Gradinaru, and P. M. Macdonald, Biomacromolecules **12**, 2364 (2011).
[5] D. Thid, J. J. Benkoski, S. Svedhem, B. Kasemo, and J. Gold, Langmuir **23**, 5878 (2007).
[6] Y. A. Domanov and P. K. G. Kinnunen, Biophys. J. **91**, 4427 (2006).
[7] K. Giger, E. R. Lamberson, and J. S. Hovis, Langmuir **25**, 71 (2009).
[8] G. Charras and E. Paluch, Nat. Rev. Mol. Cell Biol. **9**, 730 (2008).
[9] P. Sens and N. Gov, Phys. Rev. Lett. **98**, 018102 (2007).
[10] E. Morris and U. Homann, J. Membr. Biol. **179**, 79 (2001).
[11] P. S. Swain and D. Andelman, Phys. Rev. E **63**, 051911 (2001).
[12] A continuous lipid bilayer behaves as a semipermeable barrier between two osmotic media. However, at long time scales, there may be an exchange of osmolites through pores or edges of the supported bilayer.
[13] I. Derenyi, G. Koster, M. van Duijn, A. Czovek, M. Dogterom, and J. Prost, Lect. Notes Phys. **711**, 141 (2007).
[14] R. Lipowsky, Faraday Discuss. **161**, 1 (2012).
[15] With significant bilayer asymmetry, numerical simulations show that inflated protrusions adopt complex morpholo gies such as pearled tubes, not observed under the con ditions studied here.
[16] See Supplemental Material at http://link.aps.org/supplemental/10.1103/PhysRevLett.110.028101 for de tails of the theory, Figs. S1 S5, and a movie of the nucleation and elongation of a protrusion at $v = 1.05$. The color map represents the lipid density asymmetry $\phi^+ \quad \phi$.
[17] M. Rahimi and M. Arroyo, Phys. Rev. E **86**, 011932 (2012).
[18] The distance between the protrusions is determined pre sumably by the friction between the bilayer and the substrate and by a lower membrane adhesion at preexist ing irregularities on the PDMS surface.

[19] The conventional reduced volume of the protrusion alone, $6\sqrt{\pi}(V \quad V_0)/(S \quad S_0)^{3/2} = (6t_0/R_0)(\upsilon \quad 1)/\varepsilon_C^{3/2}$, characterizes quite well the stress and aspect ratio of the protrusions, except for small volumes or strains.
[20] T. Ursell, A. Agrawal, and R. Phillips, Biophys. J. **101**, 1913 (2011).
[21] I. Reviakine and A. Brisson, Langmuir **16**, 1806 (2000).
[22] O. Rossier, D. Cuvelier, N. Borghi, P. Puech, I. Derenyi, A. Buguin, P. Nassoy, and F. Brochard Wyart, Langmuir **19**, 575 (2003).
[23] P. V. Bashkirov, S. A. Akimov, A. I. Evseev, S. L. Schmid, J. Zimmerberg, and V. A. Frolov, Cell **135**, 1276 (2008).
[24] K. Olbrich, W. Rawicz, D. Needham, and E. Evans, Biophys. J. **79**, 321 (2000).
[25] J. C. Mathai, S. Tristram Nagle, J. F. Nagle, and M. L. Zeidel, J. Gen. Physiol. **131**, 69 (2008).
[26] Y. Li, R. Lipowsky, and R. Dimova, Proc. Natl. Acad. Sci. U.S.A. **108**, 4731 (2011).
[27] L. L. Norman, J. Brugués, K. Sengupta, P. Sens, and H. Aranda Espinoza, Biophys. J. **99**, 1726 (2010).
[28] B. Antonny, Annu. Rev. Biochem. **80**, 101 (2011).
[29] R. Dimova, S. Aranda, N. Bezlyepkina, V. Nikolov, K. A. Riske, and R. Lipowsky, J. Phys. Condens. Matter **18**, S1151 (2006).